MOLECULAR SIMULATION
2025, VOL. 51, NO. 3, 188–205
https://doi.org/10.1080/08927022.2025.2467834

Taylor & Francis
Taylor & Francis Group

Development of a coarse-grained model for the early stages of ordered mesoporous silica formation

Tom Stavert[a], Siddharth V. Patwardhan[b] and Miguel Jorge[a]

[a]Department of Chemical & Process Engineering, University of Strathclyde, Glasgow, UK; [b]Department of Chemical and Biological Engineering, University of Sheffield, Sheffield, UK

ABSTRACT

Understanding the early stages of the synthesis of ordered mesoporous silica materials is not only incredibly important to control the nanoporous structure of the material that forms, but can also inform the design of sustainable manufacturing. Computational modelling is an invaluable tool to study this process, enabling a move away from trial and error experimental studies towards a more rational computer-aided design procedure for these valuable nanomaterials. However, this is made challenging by the complexity of the self-assembly process that governs the early stages of synthesis, which takes place over a broad range of time and length scales that are inaccessible to current traditional atomistic models. In this work, a coarse-grained molecular dynamics model based on the Martini 3 force-field is developed following a systematic multi-scale strategy that can also be adopted for many similar systems which rely on a delicate balance of interactions between inorganic precursor species and a surfactant template. Self-assembly results with the new model are consistent with available experimental data on these systems.

ARTICLE HISTORY
Received 9 October 2024
Accepted 11 February 2025

KEYWORDS
Porous silica; self-assembly; surfactants; molecular simulation; multi-scale model

1. Introduction

Since their discovery in the 1990s [1], ordered mesoporous silica (OMS) materials (such as MCM-41 and SBA-15) have generated a great deal of attention due to their diverse range of potential applications including drug delivery, gas separation, catalysis and sensors [2,3]. The synthesis of these nanoporous materials hinges on the formation of an ordered liquid crystal mesophase, which occurs via the co-operative self-assembly of surfactant and silica precursor species. Since the morphology of OMS is determined by this self-assembly process, understanding the formation of the liquid crystal phase allows for prediction of the structure of the resultant porous material, creating a crucial link between synthesis conditions and material properties. Many experimental studies have attempted to understand the mechanisms of self-assembly using a broad variety of techniques including in situ x-ray and neutron scattering [4]. However, due to the complexity of the synthesis process, which involves a range of phenomena including self-assembly, chemical reactions, nucleation and phase separation taking place simultaneously over a broad range of time and length scales, it is a challenging system to probe experimentally. Therefore, a variety of computational modelling techniques have been applied to study this system, which have been extensively reviewed elsewhere [5].

One successful technique made use of highly coarse-grained lattice models which were tuned to reproduce the underlying interactions that give rise to self-assembly in MCM-41 synthesis [6,7], and were able to demonstrate the phase separation into a concentrated, hexagonally ordered silica/surfactant phase and a dilute aqueous phase. The model was later extended to explicitly account for silica polymerisation reactions, which showed that allowing silica condensation to occur too early in the self-assembly process resulted in a disordered amorphous silica rather than an ordered hexagonal liquid crystal (HLC) phase [8]. Despite these successes, the simplifications inherent in lattice-based models make it difficult to retain chemical specificity (e.g. a lattice model for a surfactant can represent a number of different chemical species) and hence to make direct connections with experimental systems.

Another fruitful approach followed a multi-scale strategy, using atomistic models of silica and surfactant species to tune coarse-grained (CG) molecular dynamics models using the Martini 2 framework [9,10]. In the work of Pérez-Sánchez et al. the first silicate species that were modelled were neutral and anionic monomers ($Si(OH)_4$ and $Si(OH)_3O^-$). When larger systems were simulated using the CG model, the presence of anionic silica monomers was found to promote the formation of large rodlike micelles rather than discrete spherical micelles. It was proposed that this was due to charge screening by the silicate species [9]. In atomistic simulations, anionic dimer species around a single CTAB micelle aggregated primarily outside of the headgroup of the micelles rather than being absorbed inside, which promoted micelle aggregation.

CONTACT Miguel Jorge miguel.jorge@strath.ac.uk
Supplemental data for this article can be accessed online at http://dx.doi.org/10.1080/08927022.2025.2467834.

The CG model showed that the formation of a hexagonal mesophase, reminiscent of OMS materials such as MCM-41, was only possible when the concentration of dimers (as a percentage of total silicate species) was over 33%, in agreement with experimental observations [11]. This observation was used to suggest that the formation of higher oligomers of silica was essential to hexagonal phase formation in MCM-41 synthesis [10]. Later work using this model explored systems with higher surfactant concentrations to investigate the formation mechanism for OMS materials. This work supported the cooperative templating mechanism for MCM-41 and MCM-48 materials, but could not rule out the liquid crystal templating mechanism for MCM-50 at very high surfactant concentrations [12].

The system modelled by Pérez-Sánchez et al. involves silicate species, the cationic surfactant cetyltrimethylammonium bromide (CTAB) and water. First, the model for CTAB was validated with a binary CTAB and water system, comparing average micelle size and surfactant aggregation number to experimental data. Next, the model for anionic silica monomers was developed using a comparison between CG simulations and an atomistic reference [9]. The atomistic model used as a reference for anionic silicates was the model of Jorge et al. [13,14] which was adapted from the neutral silicates model of Pereira et al. [15] with new charges and geometries obtained from DFT calculations [16]. This CG model was later extended to include higher oligomers of anionic silica, namely dimers, linear trimers and tetramers, cyclic trimers and tetramers, and cubic octamers [10]. In these higher oligomers, one CG bead is used per silicon atom and the same parameters are used for all beads in all oligomers with the exception of cyclic oligomers, which used the same bead type but with an 'S' (meaning small) prefix, thus changing interactions with other small beads. However, in Martini 2, interactions between small beads and regular sized beads are unchanged when this prefix is applied. It should be noted, however, that the parameters used for higher oligomer beads are different from those used for monomers. This is because in atomistic simulations of a single CTAB micelle, the silica monomers were absorbed into the headgroup of the micelle whereas the dimers aggregated primarily outside the headgroup region. Therefore, the parameters of dimers were adjusted from the original monomer model to reproduce this behaviour. This model was then used to study the behaviour of ternary CTAB/water/silica systems at higher concentrations [12].

As mentioned above, the model of Pérez-Sánchez et al. was built using the Martini 2 force field [17]. This is a 'building block' based force field where four heavy (non-hydrogen) atoms are mapped to each bead on average, based on their chemical specificity. Martini 2 is an incredibly popular force field with a broad range of applications. However, it has certain limitations. In particular, it lacks cross interactions between beads of different sizes and provides poor agreement with experimental data for both solutes and solvents where short bond lengths are used [18].

In recent years, the Martini 3 force field has been published which aims to fix some of the issues with the previous version whilst also expanding the range of bead types available [19]. Martini 3 follows the same 'building block' methodology where, on average, 4 heavy atoms are represented by a single 'bead'. However, Martini 3 also provides specific interactions for 'small' and 'tiny' bead types which typically represent 3 and 2 heavy atoms, respectively, allowing for the chemical specificity of small groups to be represented more easily with higher resolution mapping. Critically, these beads also have specific cross-interactions between different sizes, allowing for improved intermolecular interactions and packing. Martini 3 has 29 available bead types versus the 18 available in Martini 2, and uses 21 discrete interaction levels between different beads versus the 10 used in Martini 2. In addition, Martini 3 introduces 'labels' which can be applied to beads to represent properties like hydrogen bonding capabilities or partial charges. This, in theory, should allow for the accurate representation of a broader range of chemical species in Martini 3 than was possible in Martini 2.

The availability of the Martini 3 force-field [19] and of a new force-field for atomistic simulation of silicate species [20] presents an opportunity to improve upon the CG model for OMS formation of Pérez-Sánchez et al. [10]. The new atomistic model for silicates, recently developed by Jorge et al. [20], was parametrised according to the Polarisation Consistent Approach (PolCA) [21,22] and validated against available experimental data for organosilicates. The availability of this improved model motivates the need to re-parametrise any CG model used in this work to ensure that it is validated against the most up-to-date atomistic models for silicates. In addition, the increased degree of customisation built into the Martini 3 force-field when compared to the previous iteration in terms of additional bead types, sizes and labels, allows for the CG model to be more finely tuned to match data from both experiment and more detailed (i.e. atomistic) simulations, permitting finer control over the interactions in the system that give rise to OMS formation. Furthermore, the use of the Martini 3 model provides an improved ability to incorporate additional species into the system. By creating a model using the Martini 3 force-field it is possible to take advantage of the improvements in representing these additional species, and compatibility with future models for species relevant to mesoporous silica formation (e.g. additives, surfactants, co-surfactants) is ensured. For these reasons, we adopt the Martini 3 framework in this work, which implies that the models for all molecules need to be re-developed and/or revalidated.

2. Methodology

2.1. Modelling approach

In this work, a similar procedure to that presented by Pérez-Sánchez et al. [9] has been applied to develop the CG model under the Martini 3 framework. This involves first validating a model for CTAB, then extending this model to include silicates. The approach used for validation will depend upon the availability of either experimental data or atomistic level models for a particular chemical species. For CTAB, the experimentally determined aggregation number and phase behaviour were used to validate the coarse-grained model, similar to the approach of Pérez-Sánchez et al. [9]. Silicates are only stable in aqueous solution at very low concentration and/or very high pH as silicic acid and its derivatives. At higher

concentrations and closer to neutral pH, silicic acid precipitates as a gel [23] and therefore there are no pure-fluid experimental properties that can be used to directly validate the CG model. To circumvent this limitation, in our previous work, an atomistic model for silicates was validated against experimental data for organosilicates, such as density and enthalpy of vaporisation, since organosilicates are stable as pure liquids [20]. In the present work, the CG model for silicates is validated against this atomistic model of Jorge et al., and therefore the CG model is also indirectly validated against experimental data. Therefore, for all new species modelled, a combination of 'top-down' and 'bottom-up' approaches is employed, increasing our confidence in the model to accurately predict real molecular level behaviour.

Silicates are present in solution at varying degrees of oligomerisation (i.e. monomers, dimers, trimers etc.). Therefore, the model ideally needs to be able to represent these different oligomers. However, anionic silica dimers have been shown to be sufficient for representing the self-assembly of the HLC phase in prior work [10] and therefore the development of an accurate model for silica dimers is prioritised in this work. As in the work of Pérez-Sánchez et al., dimer parameters are thereafter assumed to be valid for higher oligomers; we will analyse the validity of this assumption later in the paper. For dimers, the first two pKa values which correspond to the deprotonation of a single silanol group bonded to each silicon atom have been reported as 9.0 and 10.7, while the pKa value corresponding to the first deprotonation of a silanol group in silica monomers is 9.5 [24]. The relative composition of the different degrees of protonation for dimers between pH 7 and 14 is given in Figure 1. Species with more than a single deprotonated silanol group per silicon atom are present only at extremely high pH values [24]. Thus, they are not present in significant quantities in the self-assembly of OMS materials, which typically occurs below pH 14, and are therefore not considered here.

In this work the following nomenclature for describing silicate species is used: anionic silica is identified as 'SI' while neutral silica is identified as 'SN'. This is followed by a number indicating the degree of condensation of the silica molecule (i.e. the number of silicon atoms), for example 'SI1' for anionic silica monomers and 'SN2' for neutral silica dimers. For oligomers with three or more silicon atoms, a suffix label is used to indicate the structure: l for linear molecules, y for cyclic molecules and c for cubic molecules (as in silica octamers, which are known to be present in high concentrations in OMS precursor solutions [11]). For example, anionic cyclic trimers are named 'SI3y' while anionic cubic octamers are labelled 'SI8c'. Silica oligomers with both anionic and neutral groups are labelled with the number of anionic groups followed by the number of neutral groups, followed by a label indicating structure where applicable. For example, dimers with a single deprotonated silanol group (therefore bearing a −1 overall molecular charge) are identified as 'SISN' while cubic octamers with a −4 charge are identified as 'SI4SN4c'.

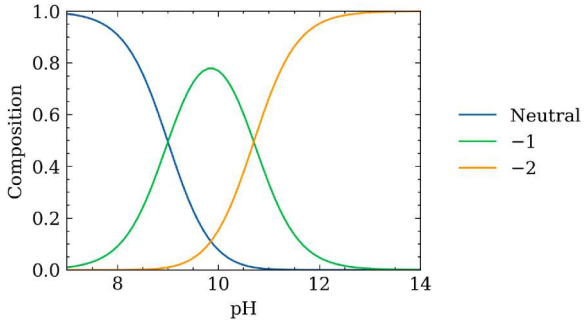

Figure 1. (Colour online) Distribution of charge states for silica dimers between pH 7 and 14. The total molecular charge for each degree of protonation is given in the legend.

A straightforward 'building blocks' based approach is suggested by the authors of the Martini 3 force-field describing how new molecules should be parametrised under this framework [19]. The procedure follows these steps, which are described in more detail below:

(1) Atomistic model is mapped to the CG beads
(2) Assign (first guess) bead types
(3) Generate bonded parameters from atomistic reference data
(4) Validate and refine bead type if required

As described previously, each Martini 'bead' represents a number of atoms, with on average 4 heavy atoms being described by each bead ('4-1 mapping'). Atoms in the molecule must therefore be divided up into groups, taking care to avoid splitting chemical groups between beads. Where it is necessary to create a group of less than 4 heavy atoms, small or tiny beads can be used to represent 3 or 2 atoms, respectively. In addition, fully branched structures and aliphatic rings should typically use a smaller bead type than linear structures. For example, a fully branched structure representing 4 heavy atoms should use a small bead instead of a regular sized bead. Higher resolution (i.e. 3-1 or 2-1) should also be considered in cases where chemical groups with different behaviours would otherwise be mapped to the same bead, as this allows for better reproduction of site-specific molecular interactions.

When the molecule is fully mapped, each bead must be assigned a 'type'. In total there are 29 different bead types available in Martini 3, including a special bead type for water. The bead types are grouped into the following categories; polar (P), intermediate/non-polar (N), apolar (C), halo-compounds (X), monovalent ions (Q), divalent ions (D), water (W). The bead type chosen determines that bead's interactions with other beads in the system through a matrix using 21 discrete interaction levels from 'hyper attractive' to 'super repulsive'. These interactions can be tweaked further with the use of 'labels' as described previously. The authors of Martini 3 also provide suggested bead types for common chemical groups, for example the C1 bead type is suggested for linear alkanes while the P5 bead type is suggested for primary amides. The selection of bead types is critical to the function of the CG model and will often need to be revised during the development and validation of the model.

Once a sensible bead type is selected, bond lengths, angles, dihedrals and their corresponding force constants need to be determined. This should be done according to the centre-of-geometry of each bead and can be calculated from an atomistic reference simulation. This can be done easily using

PyCGTOOL [25] by supplying an atomistic simulation trajectory of a single molecule in water and the mapping scheme corresponding to the molecule to be mapped.

All computational work was carried out using the GROMACS 2022.1 software package, which allows molecular dynamics (MD) simulations to be carried out with high computational efficiency due to the use of state-of-the-art algorithmic optimisations and parallelisation [26,27]. The general purpose programming language Python 3 [28] was used to aid in setting up and running simulations. For analysis of simulation data the built-in GROMACS analysis tools were used as well as the MDAnalysis library for Python [29,30]. Graphs were generated using the Matplotlib library for Python [31].

2.2. Simulation details

For atomistic simulations, the leapfrog algorithm [32] was used with a time step of 2 fs. All simulations took place at room temperature (298 K) and pressure (1 bar) using the velocity-rescaling thermostat [33] and the Parrinello-Rahman barostat [34,35]. Cubic boxes with periodic boundary conditions were used. A 1.2 nm cut-off was used for Lennard-Jones (LJ) interactions with a switching function between 0.9 and 1.2 nm. Long range dispersion corrections for both energy and pressure were applied. Electrostatic interactions were accounted for using the particle-mesh Ewald method [36,37]. Before MD for all atomistic simulations, energy minimisation was carried out using the steepest descent algorithm followed by equilibration in the NVT and NpT ensemble consecutively for 100 ps each. The rigid extended single point charge (SPC/E) potential was chosen to represent water molecules [38]. For the CTA+ cations, parameters were taken from the OPLS potential [39–44] using a fully atomistic model with explicit hydrogens. Silicates were modelled using the model of Jorge et al. [20], as described above.

Atomistic simulations were used for two purposes. Firstly, simulations of single molecules solvated in water were used to generate atomistic reference data for bonded parameters based on centre of geometry mapping. In these atomistic simulations, a single molecule was placed in a cubic box with a side length of 3 nm. The box was then solvated with an appropriate number of water molecules to achieve a realistic density using the `gmx solvate` tool in GROMACS. A simulation time of 50 ns was used for calculation of these bonded parameters. Bonded parameters were generated from simulation trajectories using the PyCGTOOL utility [25]. Secondly, atomistic simulations of a single preformed CTAB micelle were used as a reference to assess how closely the CG model matched atomistic micelle morphology, and also to validate the interactions of other molecules in the system (i.e. silicates) with the surfactant by examining their interaction with a single surfactant micelle in water. In order to evaluate this, radial density profiles for all species present in the simulations were calculated from the micelle centre-of-mass. Simulations involving a single micelle were set up starting from a pre-formed micelle used in previous work [10]. Any relevant solutes and bromide counter-ions were added randomly to the simulation box before solvation in water using the `gmx solvate` tool.

Coarse-grained simulations were carried out using the suggested parameters proposed by the authors of the Martini 3 model [19]. After setting up the initial configuration, energy minimisation was carried out using the steepest-descent algorithm. NVT equilibration was carried out using a velocity-rescaling thermostat [33] with a 2 fs time step. NpT equilibration was carried out using the Berendsen barostat, also with a 2 fs time step. Full MD simulations used a timestep of 30 fs unless otherwise stated, using the leap-frog algorithm. For temperature control, a velocity-rescaling thermostat was used and the pressure was controlled with the Parrinello-Rahman barostat [34,35]. For Lennard-Jones terms, the Verlet cutoff scheme [45] was used with a cutoff value of 1.1 nm. Electrostatics were accounted for using reaction field with a cutoff value of 1.1 nm and a relative permittivity of $\varepsilon_r = 15$.

2.3. CTAB model parameters

CTA+ is made up of 20 heavy (non-hydrogen) atoms in a linear arrangement, therefore the most straightforward mapping scheme is 5 regular size Martini beads (i.e. 4-to-1 mapping) as shown in Figure 2. The same mapping scheme was used in the model of Pérez-Sánchez et al. [9]. Linear alkanes are readily described by the C1 bead, so this bead was used for the four beads representing the alkane tail of the molecule. The charged head group is similar in nature to a tetramethylammonium cation, which is represented well in Martini 3 by a Q2 bead [19] (see Figure 2). Bonded parameters were generated from the reference atomistic model as described in 2.2 and are shown in Tables 1 and 2. The parameters generated indicate that the bond between the surfactant headgroup and first tail bead (H_1–T_2) is shorter and more rigid than bonds between surfactant tail group beads, which are slightly longer and more flexible.

For the single micelle simulation, the CG model reproduces the density profile of the atomistic simulation well (Figure 3). The micelle was stable over the simulation time, which confirms that this CG model produces stable micelles at an aggregation number of 100 surfactant molecules in agreement with the atomistic model. The density of the surfactant head and tail are similar in both the atomistic and CG model, implying that the CG model reproduces the morphology of a single micelle accurately. The modal density of the surfactant headgroup occurs at approximately 2.4 nm which can be approximated as the size of a single micelle. This is in good agreement with experimental data [46,47] and atomistic results.

2.4. Silicates

2.4.1. Atomistic simulations

Atomistic results obtained in this work for micelle radial density profiles in the presence of anionic silica monomers and dimers and neutral silica monomers are shown in Figure 4. Anionic silicates are shown to aggregate just outside of the micelle surface for all oligomers simulated. This is due to strong electrostatic interactions between the negatively charged silicate anions and the positively charged cationic surfactant headgroup. This result is in agreement with atomistic

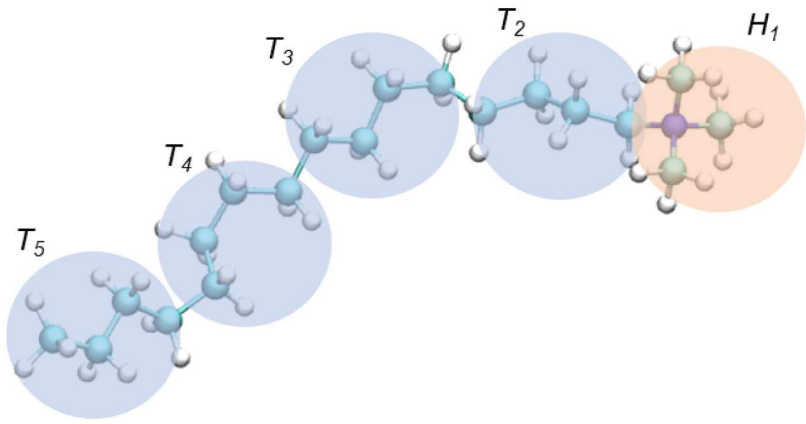

Figure 2. (Colour online) The Martini 3 mapping scheme for CTA+ cations. The beads representing the alkane tail of the surfactant are shown in blue (T_2–T_5), while the bead representing the cationic head is shown in orange (H_1).

simulations carried out in previous work for anionic dimers [10] (shown by the dotted line in Figure 4(c)). However, the result for monomers differs from previous work. In the atomistic simulations used for model validation by Pérez-Sánchez et al. (shown by the dotted line in Figure 4(a)), anionic silicate monomers were absorbed within the headgroup of the micelle whereas in this work, anionic monomers are located outside of the headgroup. This is likely to be due to the difference in the atomistic model used in this work, which results in slightly more hydrophilic silicate species.

The work of Pérez-Sánchez et al. used a silica model based on the work of Pereira et al. [15], modified according to DFT calculations [14], whereas this work employs the recently developed model of Jorge et al., which, as previously described, is validated against experimental data [20]. Thus, the atomistic results obtained in this work should be considered as a more accurate description of the behaviour of silicates. It was previously suggested that silica oligomers were required in order to bridge adjacent CTAB micelles to form the mesophase structure of MCM-41. However, this conclusion was drawn from a CG model in which monomers absorbed into the micelle surface whereas dimers aggregate on the surface outside the micelle, and therefore this behaviour will be re-examined in this work.

Neutral silicates are much more soluble in water than their anionic counterparts, remaining largely in the bulk solution as shown in Figure 4(b). This trend decreases slightly as the degree of oligomerisation increases, however. There is a small peak in the radial density profile for neutral silica monomers which sits just inside the surfactant headgroup, suggesting that a small amount of neutral silicates is absorbed within the micelle surface. A peak is also present for neutral dimers, however it sits outside the headgroup (Figure 4(d)). This may be because the higher oligomers are larger and therefore too bulky to penetrate into the micelle surface. The new atomistic model for neutral silica is clearly more hydrophilic than the atomistic model employed by Pérez-Sánchez et al. [9] (shown by the dotted line in Figure 4(b,d)), with a much larger amount of silicates present in the bulk water and only a small amount of silicates aggregating near the micelle surface.

2.4.2. Model mapping and bonded parameters

Silicate monomers (both neutral and ionic) contain five heavy atoms in a branched arrangement and therefore were mapped to a single regular size Martini bead. Dimers and trimers were modelled with two and three regular beads, respectively, splitting bridging oxygen atoms between beads in order to maintain the symmetry of the molecule (see Figure 5). A similar procedure was carried out for cyclic and cubic fragments, with beads centred on the silicon atom and bridging oxygens split between beads where necessary (see Figure 6). For beads in cyclic and cubic molecules, the small bead size should be used as per the recommendation of the Martini 3 authors [19].

To allow the CG model for silicates to represent linear oligomers of any degree of condensation and at any ionisation state, it was necessary to generate bonded parameters for each possible combination of anionic and neutral silicates. Since the CG model only requires bond and angle parameters, it is straightforward to achieve this for linear fragments with a series of simulations of trimers of differing ionisation states. From these simulations, the average bond length was calculated for each bond type and these parameters were used for all CG simulations involving linear silicates. For cyclic fragments, reference atomistic simulations were carried out for

Table 1. Bonded parameters for CTA+ Martini 3 model.

Bond	b_{ij} (nm)	k_{ij} (kJ mol^{-1})
H_1–T_2	0.375	39,000
T_2–T_3	0.478	3450
T_3–T_4	0.478	3450
T_3–T_5	0.483	3450

Note: Bead names refer to labels in Figure 2. b_{ij} is the bond length and k_{ij} is the bond force constant.

Table 2. Angle type parameters for CTA^+ Martini 3 model.

Beads	θ_{ijk} (degrees)	Calculated k_{ijk} (kJ mol^{-1})
H_1–T_2–T_3	156	180
T_2–T_3–T_4	150	100
T_3–T_4–T_5	150	100

Note: Bead names refer to labels in Figure 2. θ_{ijk} is the angle between beads and k_{ijk} is the angle force constant.

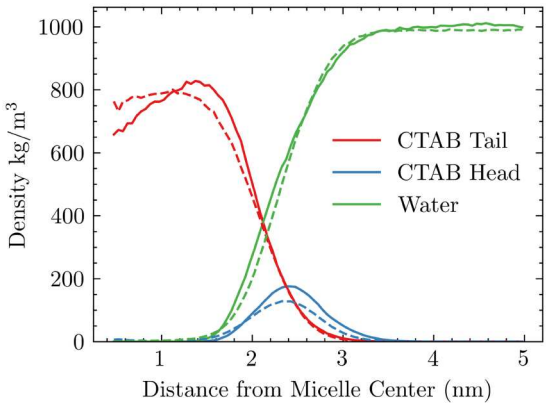

Figure 3. (Colour online) Comparison of single micelle density profiles for atomistic (filled lines) and CG simulations (dashed lines), calculated from the micelle centre of mass. The density profiles of bromide counter-ions are hidden for clarity.

fully deprotonated cyclic trimers and cubic octamers. These bonded parameters are given in Tables 3 and 4.

When using the larger timesteps of circa 30 fs, which are frequently employed using the Martini model, high bond force constants ($> 30{,}000\,\mathrm{kJ\ mol^{-1}}$), representing very stiff bonds, can cause the oscillation of the bond to be much faster than the simulation timestep. This can cause issues with energy conservation and the numerical stability of simulations. There are two approaches that could ideally be applied to handle this situation. The first is to reduce the simulation timestep to improve stability, however this has obvious and unacceptable impacts on the computational cost of simulations. The second is to instead treat these bonds as rigid by using a constraint algorithm, such as the LINear Constraint Solver [48]. This is practical in some circumstances, however large numbers of constraints, particularly when they are interconnected (as would be the case in cyclic fragments) can cause instabilities as identified by the authors of the Martini 3 force-field [19]. Some unique approaches have been demonstrated to reduce the number of constraints required for describing stiff cyclic molecules, such as the hinge model of Melo and co-workers used for sterols and hopanoids [49]. However, this approach adds additional complexity to model development and is not compatible with the objective of creating a general model capable of representing larger silica oligomers whilst retaining numerical stability. Therefore, the approach taken in this work is to compromise strict agreement with atomistic reference data in favour of numerical stability. For all silicates, force

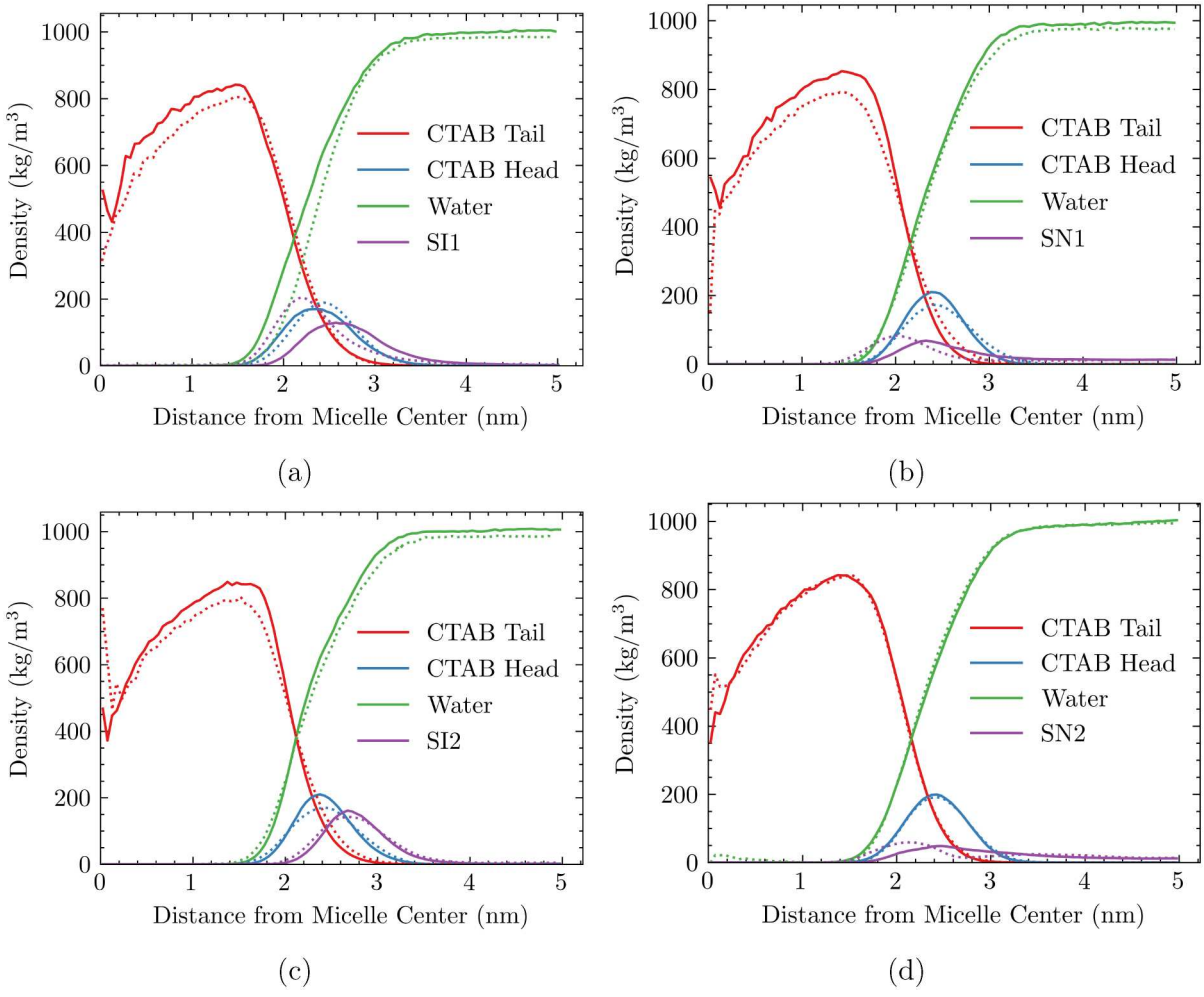

Figure 4. (Colour online) Time averaged radial density profile of single micelles in the presence of anionic silicate monomers (a) and dimers (c) and neutral silicate monomers (b) and dimers (d). Results obtained in the work of Pérez-Sánchez et al. [9] are shown by dotted lines, while the results obtained here using the new atomistic model of Jorge et al. [20] are shown by filled lines.

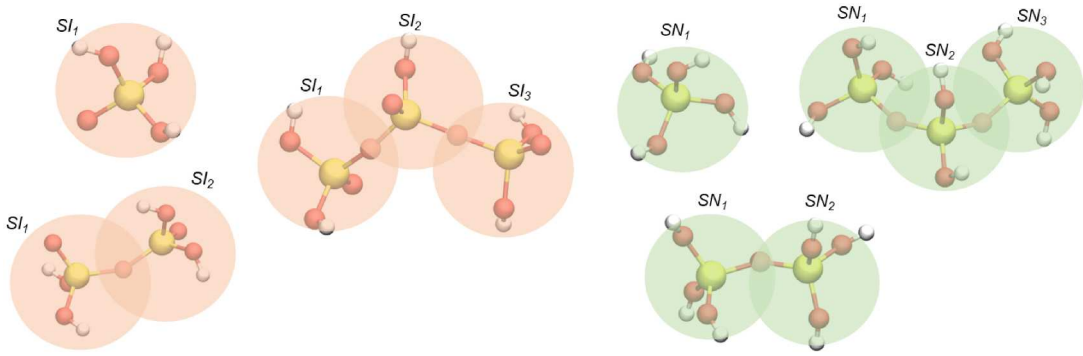

Figure 5. (Colour online) Martini 3 mapping scheme for neutral (green) and anionic (red) silicates showing monomers, dimers and linear trimers.

constants greater than 30,000 kJ mol^{-1} were reduced to 30,000 kJ mol^{-1}. While the equilibrium bond length remains unchanged, this significantly improves numerical stability at larger timesteps (30 fs) whilst still retaining an element of bond rigidity.

Cubic octamers present an additional difficulty as the large number of bonds in an interconnected network make achieving numerical stability difficult, even with a reduction in the force bond constant to 30,000 kJ mol^{-1}. Therefore, the force constant of this bond was significantly reduced to 1250 kJ mol^{-1} and in addition the angle force constant is relaxed to 25 kJ mol^{-1} to further improve numerical stability.

For simplicity, protonation states were not considered for cyclic oligomers, assuming the bonded parameters between neutral silicate beads in a cubic or cyclic arrangement are the same as the bonded parameters for anionic silicate beads. The bond lengths and angles in these oligomers were averaged to give a single bond length and angle for cyclic and cubic segments.

2.4.3. Bead type selection

Initially an attempt was made to select a bead type to represent silicates from the standard bead types available in Martini 3. For anionic silicates, all available charged (Q) bead types were tested and for neutral silicates, various N (neutral) bead types were tested. Ideally, the same bead type should be used for segments of silica oligomers as is used for silica monomers, as this permits the simulation of oligomers of any length without the need to parametrise the model again for each different oligomer. The initial goal is therefore to choose a bead for each ionisation state of silica (neutral and anionic) that is capable of representing multiple oligomerisation states of silica with reasonable accuracy.

First, simulations involving monomers and dimers were compared against atomistic data generated as described in Sections 2.4.1 and 2.4.2. There are several approaches that can be taken to assess the comparison between CG and atomistic data. Perhaps the most straightforward method is to directly compare the silica radial density profile generated from CG simulations with the silica radial density profile generated from atomistic simulations. This comparison is displayed in Figure 7. For anionic silicates, all bead types produced qualitatively similar radial density profiles for silica with a region of high silicate concentration close to the micelle surface. To quantitatively describe the peaks, the peak density value and corresponding radial distance from the micelle centre were determined (see Table S1). From these results, it is clear that there is a balance to be struck when deciding on a bead type to match both the peak height and location of the atomistic reference data.

While the behaviour of silica monomers and dimers is quite similar in atomistic models, there is a large difference in behaviour between equivalent bead types in the CG model. In general, CG simulations of silica monomers result in silica density profiles that indicate more hydrophilic character than is present in the atomistic model, with a higher concentration of silicates present in the bulk solution (> 4 nm from micelle centre). In contrast, CG simulations of silica dimers result in silica density profiles that more closely match atomistic data, with a larger quantity of silicates aggregating close to the micelle surface. This suggests, firstly, that the standard Martini 3 bead types are not ideal for representing anionic silica monomers and, secondly, that the best bead type used for representing monomers may not scale well to higher oligomers of silica using the Martini 3 model. Therefore, it was decided to select different bead types for silica monomers and dimers, with the choice for dimers being more likely to scale well to higher oligomers of silica.

However, direct comparison of the silica density in isolation does not give a complete picture of the quality of the fit between atomistic and CG simulation data. This is illustrated in Figure 8, which shows the complete density profile of all species present in simulations involving silica dimers for Martini 3 charged bead types Q1 and Q5. Comparing the relative heights of the peaks for the CTAB headgroup and silicates for these bead types, one can see that for both CG simulations surfactant headgroup peaks are shorter and wider than in the atomistic reference. This has an effect on the silica peak, which follows a similar behaviour. Thus, it can be argued that consideration of the full profile of all species (in particular the surfactant headgroup and silica densities) is important to determining the best fit. However, from simply examining the profiles visually (as was done in previous work [9,10]) it is difficult to draw distinctions between bead types, leading to a subjective choice of which bead type is most suitable.

Since a subjective assessment of the quality of fit between CG and atomistic data is not a robust method for model development, it is desirable to develop a more thorough procedure

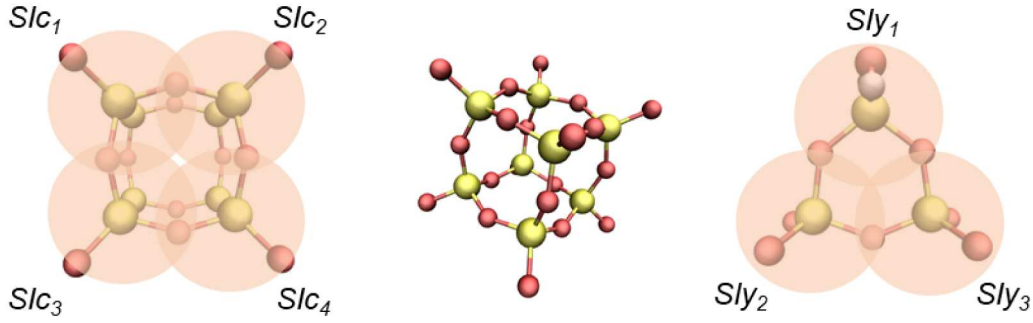

Figure 6. (Colour online) Martini 3 mapping scheme for cyclic silica oligomers. For cubic oligomers, the mapping scheme is displayed for the front face (leftmost image), for which there is a symmetrical arrangement on the back face (up to SIc_8).

for comparing silica and surfactant interactions for simulations involving a single micelle in order to provide an objective measure for bead type selection which can also be more generally applied to other systems, particularly those that involve co-operative self-assembly. As such, the following fitting parameters were devised based on the results of single micelle systems (see Figures S2 and S3 in Supporting Information for all individual density profiles).

The first fitting parameter, H, is based on the relative peak heights of the surfactant headgroup and silicate species in the single micelle radial density profile:

$$H = \frac{\left(\frac{h_{SI,CG}}{h_{H,CG}}\right)}{\left(\frac{h_{SI,A}}{h_{H,A}}\right)} \quad (1)$$

where h represents the peak height in the radial density profile with the subscript representing the species and type of simulation (atomistic or CG) respectively. A perfect fit gives an H value of 1 indicating that the relative heights of the surfactant headgroup and silica peaks are the same as atomistic simulations. To assess the fit for peak location, the fitting parameter R is used, which takes into account the relative locations (radial distance from micelle centre) where the peaks occur:

$$R = \frac{\left(\frac{r_{SI,CG}}{r_{H,A}}\right)}{\left(\frac{r_{SI,A}}{r_{H,A}}\right)} \quad (2)$$

where r is the radial distance from the micelle centre of mass where the peak occurs. A final fitting parameter, N_{ads} is proposed, which is simply based on the quantity of silica molecules that are adsorbed onto the micelle surface in CG simulations versus the atomistic reference. This figure is a simplistic measure of the relative balance between micelle surface adsorption and bulk water solubility. To determine N_{ads}, the average number of silica molecules adsorbed on the micelle surface is calculated over the simulation trajectory after equilibrium has been reached for both atomistic and CG simulations. For CG simulations, a silica molecule is considered adsorbed if any bead of it is within 0.73 nm of the CTAB headgroup bead, which is approximately the distance at which the first minimum in the radial distribution function between silicate species and surfactant headgroup is observed. For the atomistic reference simulation, the distance is calculated between each silicon atom in silicate species and the nitrogen atom in the surfactant headgroup.

$$N_{ads} = \frac{N_{ads,CG}}{N_{ads,A}} \quad (3)$$

The values of fitting parameters H, R and N_{ads} for the bead types tested are plotted in Figure 9. Firstly considering parameter H, which indicates how proportional the surfactant headgroup and silica peaks are to atomistic data, different optimum values are observed for monomers and dimers. The value of H for monomers is significantly lower than that of dimers for the same bead type. Examining the trends in the relative heights of the silica peaks for different bead types (displayed in Figure 7) it can be seen that for all bead types the silica peak height is much lower than the atomistic reference, with all bead types producing peak densities less than half the height of the atomistic reference. This indicates that all standard Martini bead types tested are too hydrophilic to represent silica monomers optimally, with a large proportion of silicates remaining in bulk water. This stands in contrast to simulations with dimers, where most bead types have a value of H>1, indicating that dimer species for these bead types are too hydrophobic, with a disproportionate quantity of silica molecules

Table 3. Bond type parameters for silica Martini 3 model.

Bond	b_{ij} (nm)	Calculated k_{ij} (kJ mol^{-1})	Model k_{ij} (kJ mol^{-1})
SI – SI	0.3500	50,000	30,000
SI – SN	0.3570	67,000	30,000
SN – SN	0.3640	75,000	30,000
SIc – SIc	0.3135	>100,000	1250
SIy – SIy	0.3330	33,000	30,000

Note: b_{ij} is the bond length and k_{ij} is the bond force constant. The calculated k_{ij} values were produced from atomistic reference simulations while the model k_{ij} values are the values actually used for the CG model.

Table 4. Angle type parameters for silica Martini 3 model.

Silica Beads	θ_{ijk} (degrees)	Calculated k_{ijk} (kJ mol^{-1})	Model k_{ijk} (kJ mol^{-1})
SI – SI – SI	102	270	270
SI – SI – SN	103	440	440
SI – SN – SI	105	400	400
SI – SN – SN	104	530	530
SN – SN – SN	102	740	740
SN – SI – SN	101	640	640
SIc – SIc – SIc	90	8874	25

Note: θ_{ijk} is the angle between beads and k_{ijk} is the angle force constant. The calculated k_{ij} values were produced from atomistic reference simulations while the model k_{ijk} values are the values used for the CG model.

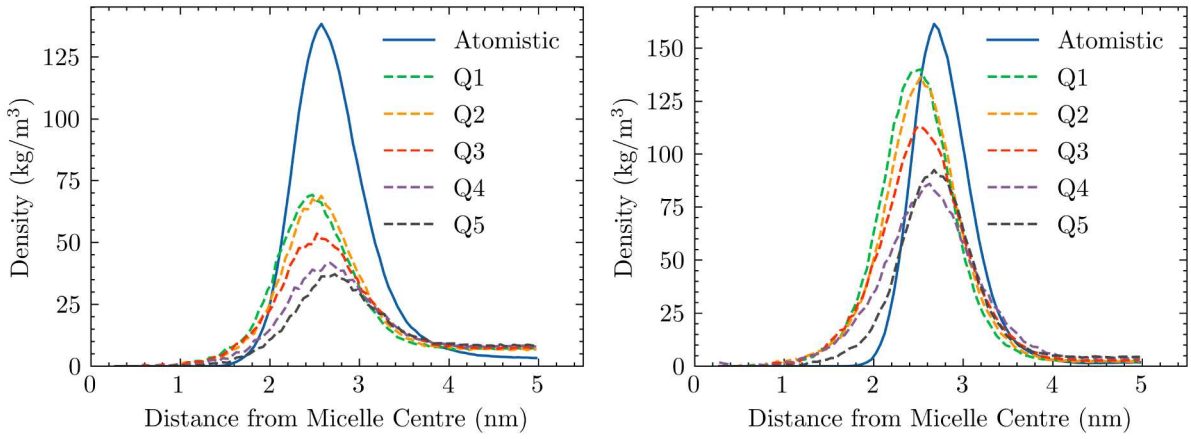

Figure 7. (Colour online) Radial density profiles for anionic silica monomers (left) and dimers (right) comparing atomistic results with various Martini 3 standard bead types.

being adsorbed onto the micelle surface. Overall, both the Q1 and Q2 bead types provide approximately equivalent fits for parameter *H* for monomers, while the Q4 bead provides a very good fit for dimers.

Now considering parameter *R*, which indicates the location at which silicate species adsorb on the micelle surface in CG simulations versus reference atomistic simulations. For monomers, the Q3 bead achieves the best fit, while for the dimers, the Q4 and Q5 beads both achieve perfect agreement with atomistic data. Finally, we consider parameter N_{ads}, which indicates the quantity of silica bound to the micelle in CG simulations versus the atomistic reference. For monomers, the value of N_{ads} was significantly below 1, once again indicating the standard Martini 3 bead types are too hydrophilic to represent silica monomers optimally. The closest agreement is once again achieved by both the Q1 and Q2 bead types, however it is worth noting that this value is still relatively low at 0.63. The standard Martini 3 bead types provide much better agreement for dimers however, with the Q3 bead achieving the best fit with atomistic data in this case.

Overall, from examination of these parameters it can be concluded that the ideal bead type for representing anionic silica dimers lies between Q3 and Q5, with Q4 providing overall the best balance between all fitting parameters. While the fit against atomistic data is generally poorer for monomers for all bead types (in particular for parameters *H* and N_{ads}), the Q1 and Q2 bead types provide the best fits out of the standard Martini 3 bead types, with either being likely to provide reasonable representation of anionic silica monomers. The Q2 bead type was favoured due to a slightly improved fit for parameter *R*. In either case, the bead type choice indicated by these parameters is different from the range identified for modelling silica dimers, which suggests that increasing the degree of condensation may alter the silica-surfactant interactions sufficiently to warrant the use of different charged bead types for larger oligomers. Indeed, the model of Pérez-Sánchez et al. employed different intermolecular interactions for silica oligomers than were used for monomers [10], setting a precedent for this approach.

The increased hydrophobicity of the Martini 3 monomer model versus the atomistic reference may be of some concern where this factor is critical to the result of future simulations. However, given that silica monomers are expected to play only a minor role in the formation of HLC phases versus multiply charged oligomers due to their inability to facilitate multidentate binding of micelles, this is less of a concern in this work. Improving the agreement of the CG model with atomistic data may be possible by scaling the hydrophobic/hydrophilic interactions of silicate species, a method adopted by Thomasen et al. to improve agreement with experimental data when using the Martini 3 force field to model flexible proteins [50]. Alternatively, the individual intermolecular parameters of the beads used for silicates could be manipulated (effectively creating a new 'Q' bead type) to develop a bespoke model. However, both of these approaches are not straightforward and are likely to hinder compatibility with other species modelled using the Martini 3 force field.

Finally, a CG single micelle simulation was carried out using trimers represented using Q4 beads. This allows us to assess the applicability of using the same bead choice for higher oligomers as is used for dimers by seeing how the atomistic agreement scales with increasing degree of condensation. Note that each silica bead in these trimers carries a negative charge (giving the molecule an overall -3 charge). As shown in Figure 10, the agreement when using the Q4 bead is reasonable, maintaining good agreement for both silica peak density location and height. However, when comparing the relative heights of the surfactant headgroup and silica peaks, the Q4 CG model appears to be slightly more hydrophobic than the atomistic model. This may suggest that as the degree of condensation for linear silicates increases, the hydrophobicity of the individual beads required to represent each segment should be reduced, as was the case when moving from silica monomers (Q2) to silica dimers (Q4). On balance, we have opted to sacrifice accuracy in favour of simplicity and transferability, and have therefore used Q4 beads to represent silicates in all anionic oligomers.

The radial density profiles generated using several different N (neutral) bead types to represent neutral silicate species are shown in Figure 11, where the silica density is compared to the atomistic reference simulation. Since there is a peak in silica density near the micelle surface, the same procedure

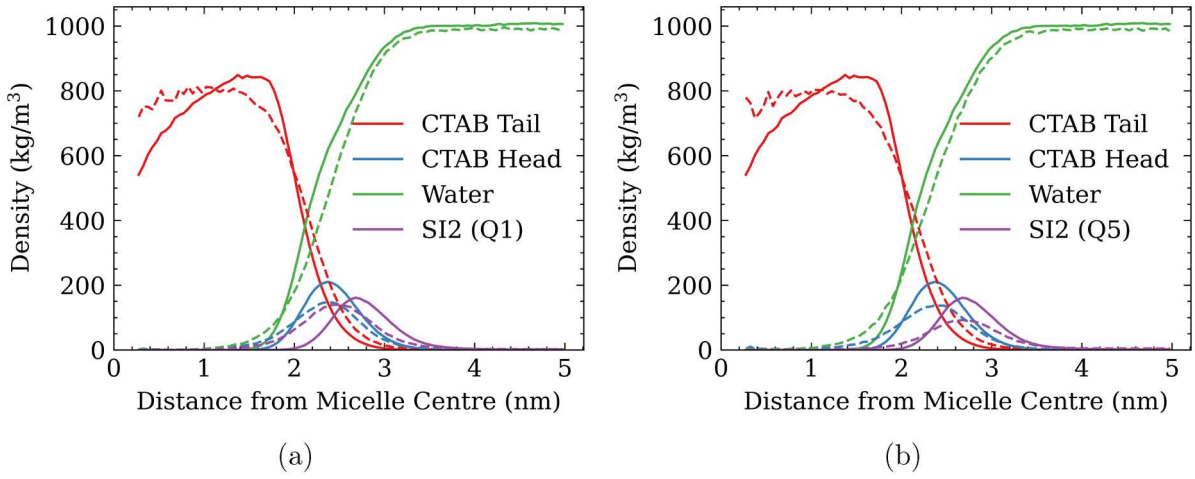

Figure 8. (Colour online) Comparison of the time averaged radial density profile around a single CTAB micelle in the presence of anionic silica dimers for the atomistic model (filled lines) and CG model (dashed lines). Silica dimers are represented using the Martini beads labelled in the legend.

employing fitting parameters H, R and N_{ads} was used to select an appropriate bead type for both monomers and dimers. These values are displayed in Figure 12. For neutral silica monomers, the N4 bead provides the best agreement with atomistic data for parameters H and R. Conversely, the N1 bead provides the best agreement for N_{ads}. However, examination of the radial density profile of silica indicates that the use of this bead type results in significant quantities of silica being absorbed within the micelle, a behaviour which is not present in the atomistic model. Therefore, the fitting of parameters H and R is prioritised, as this appears to give the most reasonable agreement with atomistic behaviour, and the N4 bead type was therefore chosen for monomers. For dimers and neutral silica fragments in higher oligomers of silica, the N5 bead was chosen as it achieves a good balance between the three fitting parameters.

The full radial density profiles for neutral silica monomers and dimers are shown in Figure 13. Both monomers and dimers show relatively good agreement with atomistic reference data, though in a similar manner to previous cases, there is a broadening and shortening of the CTAB headgroup peak. Finally, the full radial density profile for linear neutral silica trimers is shown in Figure 13(c). Here there is relatively good agreement against atomistic data, indicating that this bead type produces interactions that scale relatively well to higher oligomers of neutral silicate species.

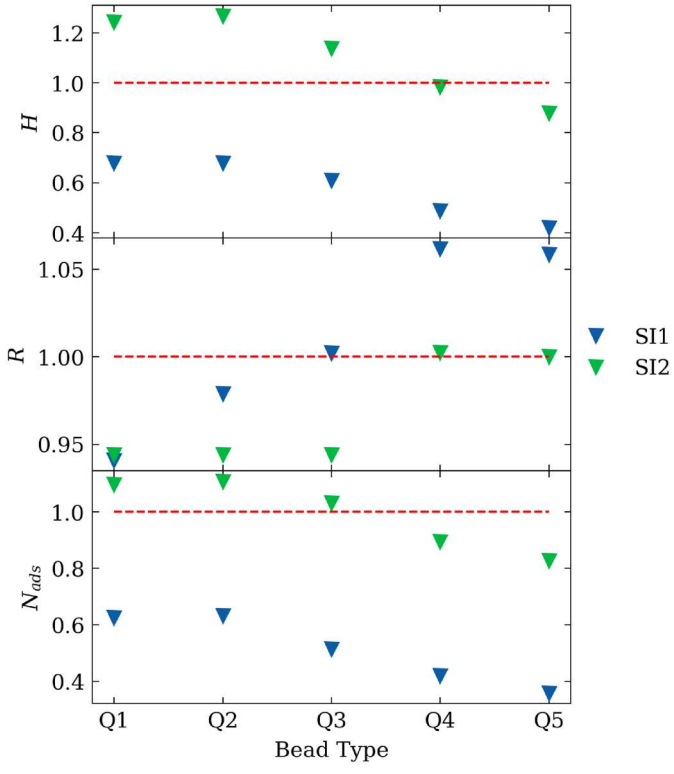

Figure 9. (Colour online) Comparison of fitting parameters for different Martini 3 bead types representing anionic silica monomers (SI1) and dimers (SI2) versus atomistic reference data. The red dashed line is a guide for the eye that indicates a perfect fit with atomistic data for each parameter.

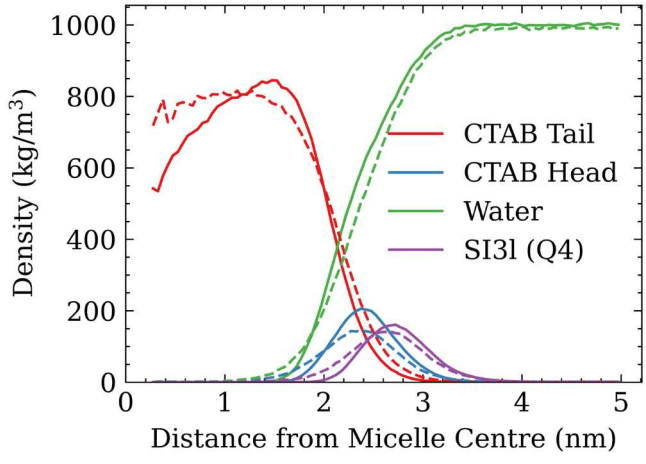

Figure 10. (Colour online) Comparison of the time averaged radial density profile around a single CTAB micelle in the presence of linear anionic silica trimers for the atomistic model (filled lines) and CG model (dashed lines). Silica trimers are represented using the Martini Q4 bead.

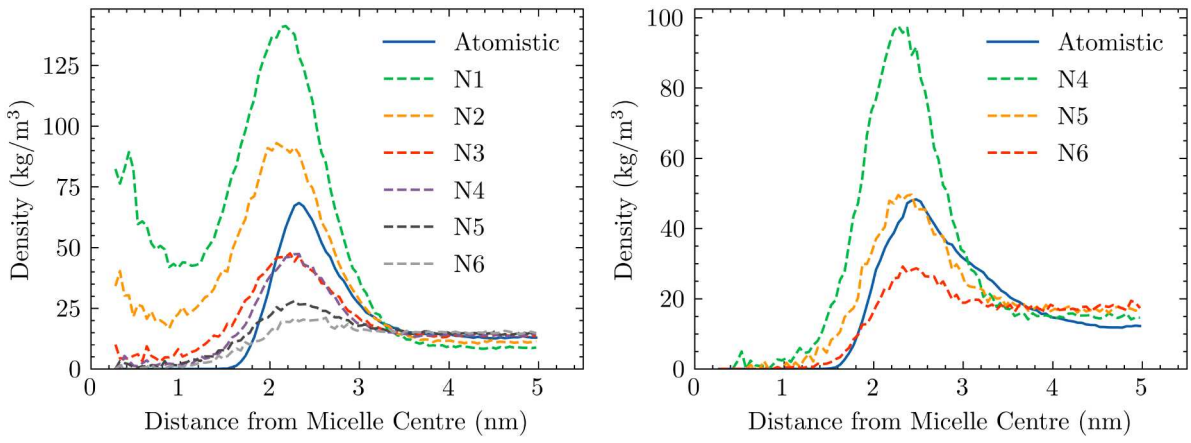

Figure 11. (Colour online) Radial density profiles for neutral silica monomers (left) and dimers (right) comparing atomistic results with various Martini 3 standard bead types.

An important aspect of the CG model is the ability to represent silica oligomers with both anionic and neutral silica units. This allows larger oligomers with a variety of charge states to be investigated, which is particularly important when considering systems at different pH values. Therefore, the model is tested by taking the simple case of a silica dimer with a single deprotonated hydroxyl group, giving the molecule an overall charge of −1. Under this model, this would be represented using one Q4 bead and one N5 bead. The bonded parameters for these mixed oligomers were also generated from atomistic data and can be found in Tables 3 and 4.

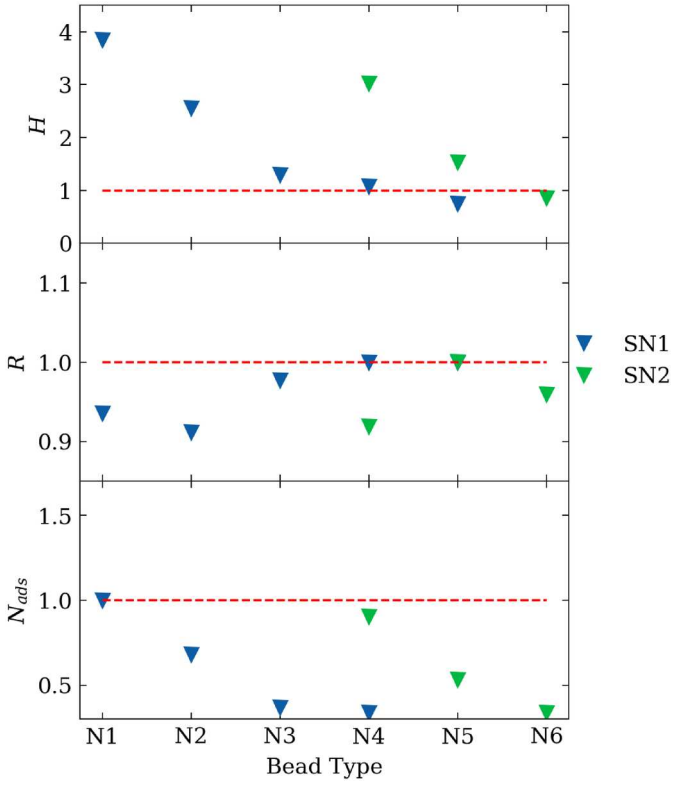

Figure 12. (Colour online) Comparison of fitting parameters for different Martini 3 bead types representing neutral silica monomers (SN1) and dimers (SN2) versus atomistic reference data. The red dashed line is a guide for the eye that indicates a perfect fit with atomistic data for each parameter.

The results of this simulation compared with an atomistic reference simulation are shown in Figure 13(d). The agreement between the atomistic reference and CG is relatively poor, with the silica peak of the CG model far less pronounced than in the atomistic model even when accounting for the broadening and shortening of the surfactant headgroup peak. This might indicate that simply mixing charged and neutral CG beads is not particularly effective at estimating the atomistic behaviour for oligomers with mixed charge states. A possible reason for this are so called 'proximity effects', which are discussed by the Martini 3 authors (supporting information of reference [19]). The interactions of a bead may be affected by their proximity to other beads, and this effect is especially pronounced for neutral beads that are connected to charged beads.

One way to account for the proximity effect of deprotonated silanol groups is to alter the bead type of beads adjacent to charged beads in oligomers. This is observed in some of the 'built-in' models present in Martini 3, such as the model for arginine which uses the SC3 bead to represent the aliphatic carbons adjacent to the charged guanidinium chemical group, which is represented by a charged bead type. The bead type typically suggested for linear alkanes is the C1 bead type (or the SC1 bead type in the case of 3 carbon atoms) and therefore the SC3 bead type is slightly more polar than the bead type that would typically be employed if following the Martini 'building blocks' approach, due to the adjacency to the very polar guanidinium group. Since the case with mixed silica oligomers is similar (i.e. a neutral bead adjacent to a polar charged group), the same technique of modifying the usual bead type to a more polar bead type could be applied, however this was not carried out in this work due to the additional complexity of the parameterisation process.

The Martini 3 bead types used in the model developed in this work for a selection of silica oligomers are displayed in Table 5. For bonded parameters, please refer to Tables 3 and 4.

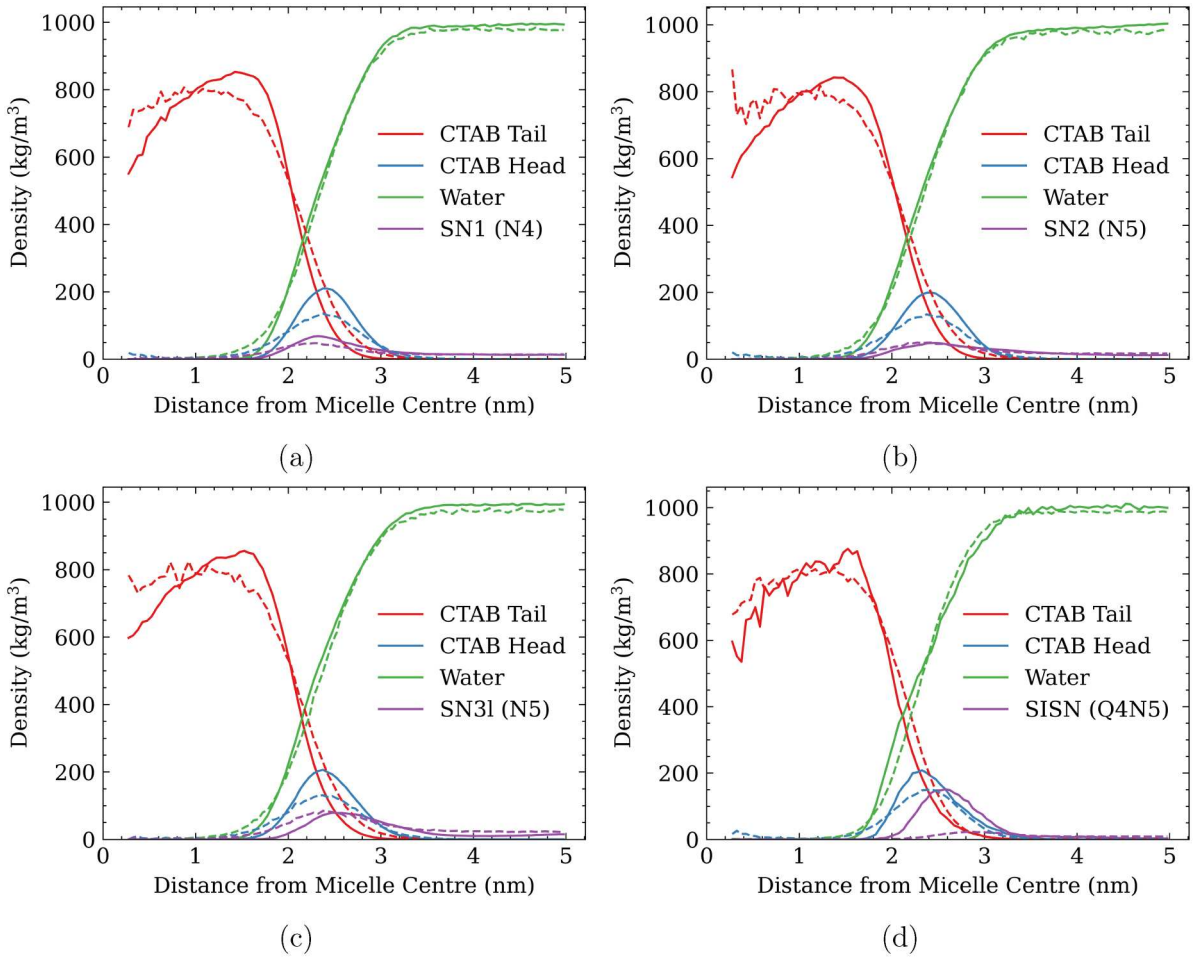

Figure 13. (Colour online) Comparison of the time averaged radial density profile around a single CTAB micelle in the presence of neutral silica monomers (a), dimers (b) and linear trimers (c) as well as singly charged dimers (d) for the atomistic model (filled lines) and CG model (dashed lines). Neutral monomers are represented using the N4 bead, while neutral beads in higher oligomers are represented using the N5 bead and charged beads are represented using the Q4 bead type.

3. Self-assembly results

3.1. CTAB solutions

CTAB self-assembly simulations at 3 and 6 wt% resulted in an average aggregation number of 125 and 167 surfactant molecules, respectively (see Figure 14, left). The experimental aggregation number for CTAB in water has been shown to increase with concentration [51,52] and experimental data from literature [46,47,51–57] is presented in Figure 14, right. It can be seen that the aggregation numbers obtained in the 3 and 6 wt% simulations agree well with the experimental trend. Snapshots of the initial and final configurations of the 6 wt% system are shown in Figure 15.

Figure 16 (right) shows visualisations of the mesophases formed after 1000 ns of simulation time for higher concentrations of CTAB. The CTAB model showed qualitative agreement with experimental observations for mesophases formed upon increasing the concentration of CTAB surfactant in an aqueous system [58]. At relatively low concentrations (15 wt%) micellar rods are formed, then upon increasing concentration first a hexagonal mesophase is formed (50 wt%), followed by a bicontinuous phase (65 wt %) and finally a lamellar phase (75 wt%). These points are plotted on the experimental phase diagram in Figure 16 (left).

Overall, the results of all CG simulations agree with both atomistic simulation results and available experimental data, suggesting that the surfactant model is suitable for reproducing surfactant behaviour.

Table 5. Examples of the bead types used in the Martini 3 model for silicates developed in this work.

Species	Charge	Nomenclature	Bead Type(s)
Anionic Silica Monomer	−1	SI1	Q2
Anionic Silica Dimer	−2	SI2	Q4
Linear Anionic Silica Trimer	−3	SI3l	Q4
Cyclic Anionic Silica Trimer	−3	SI3y	SQ4
Cubic Anionic Silica Octamer	−8	SI8c	SQ4
Neutral Silica Monomer	0	SN1	N4
Neutral Silica Dimer	0	SN2	N5
Linear Neutral Silica Trimer	0	SN3l	N5
Cyclic Neutral Silica Trimer	0	SN3y	SN5
Cubic Neutral Silica Octamer	0	SN8c	SN5
Mixed Silica Dimer	−1	SISN	Q4/N5
Mixed Silica Octamer	−4	SI4SN4c	SQ4/SN5

Note: The bead type listed is used in each unit of the oligomer or in the case of mixed oligomers in each anionic/neutral unit, respectively.

3.2. CTAB/silica solutions

After initial calibration against the atomistic model for silicates, validation of the bead type selection is carried out by

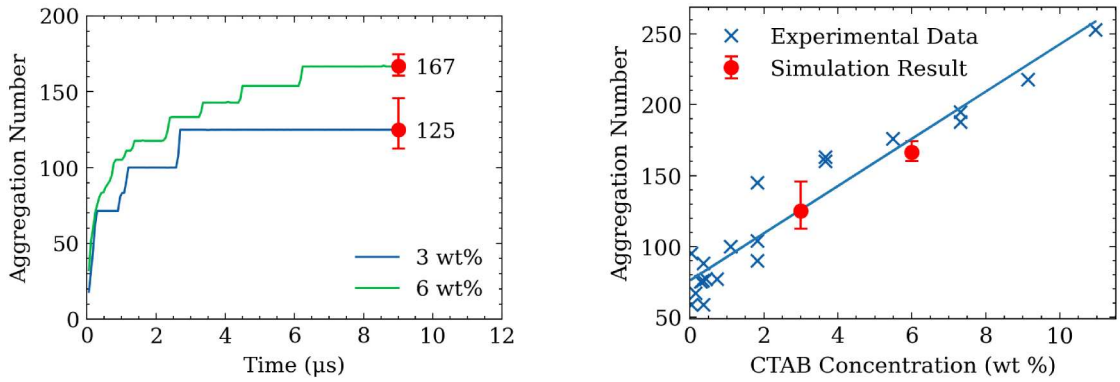

Figure 14. (Colour online) On the left, a graph is presented for the aggregation number during self-assembly simulation using CG model for CTAB at 3 and 6 wt%. On the right, the experimental aggregation numbers for CTAB are plotted at various concentrations with data taken from [46,47,51–57]. The final aggregation number obtained in the simulations is shown by red circles.

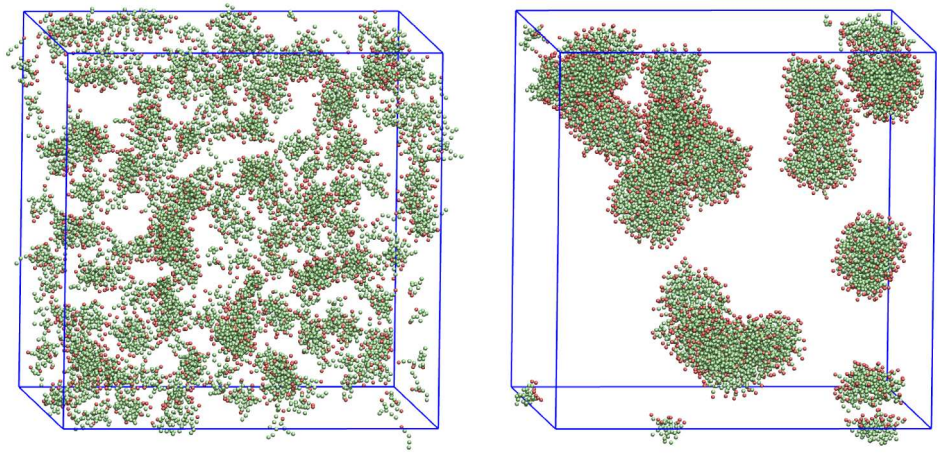

Figure 15. (Colour online) Simulation snapshots of the 6 wt% CTAB system, showing the initial configuration (left) and final configuration (right) after 9 μs of simulation time. CTAB head group beads are shown in red and tail group beads are shown in green. Bromide counter-ions and water are hidden for clarity.

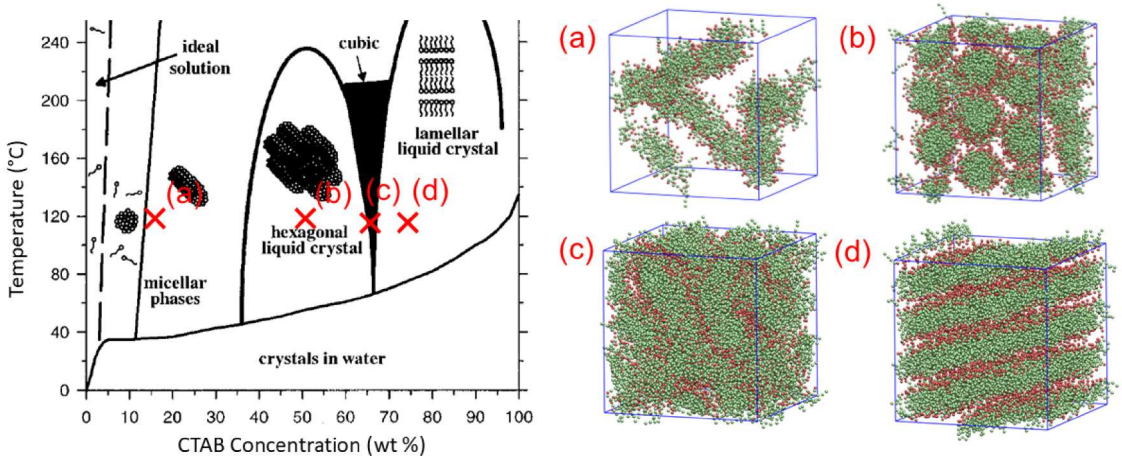

Figure 16. (Colour online) Phase diagram for CTAB in water showing the experimentally observed liquid crystal phases at a range of surfactant concentration and temperature values (adapted from [59]). Simulation snapshots of points labelled on the diagram are shown on the right, with (a) showing a micellar phase, (b) showing a hexagonal liquid crystal phase, (c) showing a bicontinous phase and (d) showing a lamellar phase. In snapshots, surfactant heads are shown in red while surfactant tails are shown in green. Water and bromide counter-ions are hidden for clarity.

studying the self-assembly behaviour of the ternary silica/surfactant/water system, and comparing this with expected behaviour from experiments and previous simulation studies. Simulations are carried out with different speciation of silica (degree of condensation and ionisation states) with different expected behaviour in each case. For this initial validation,

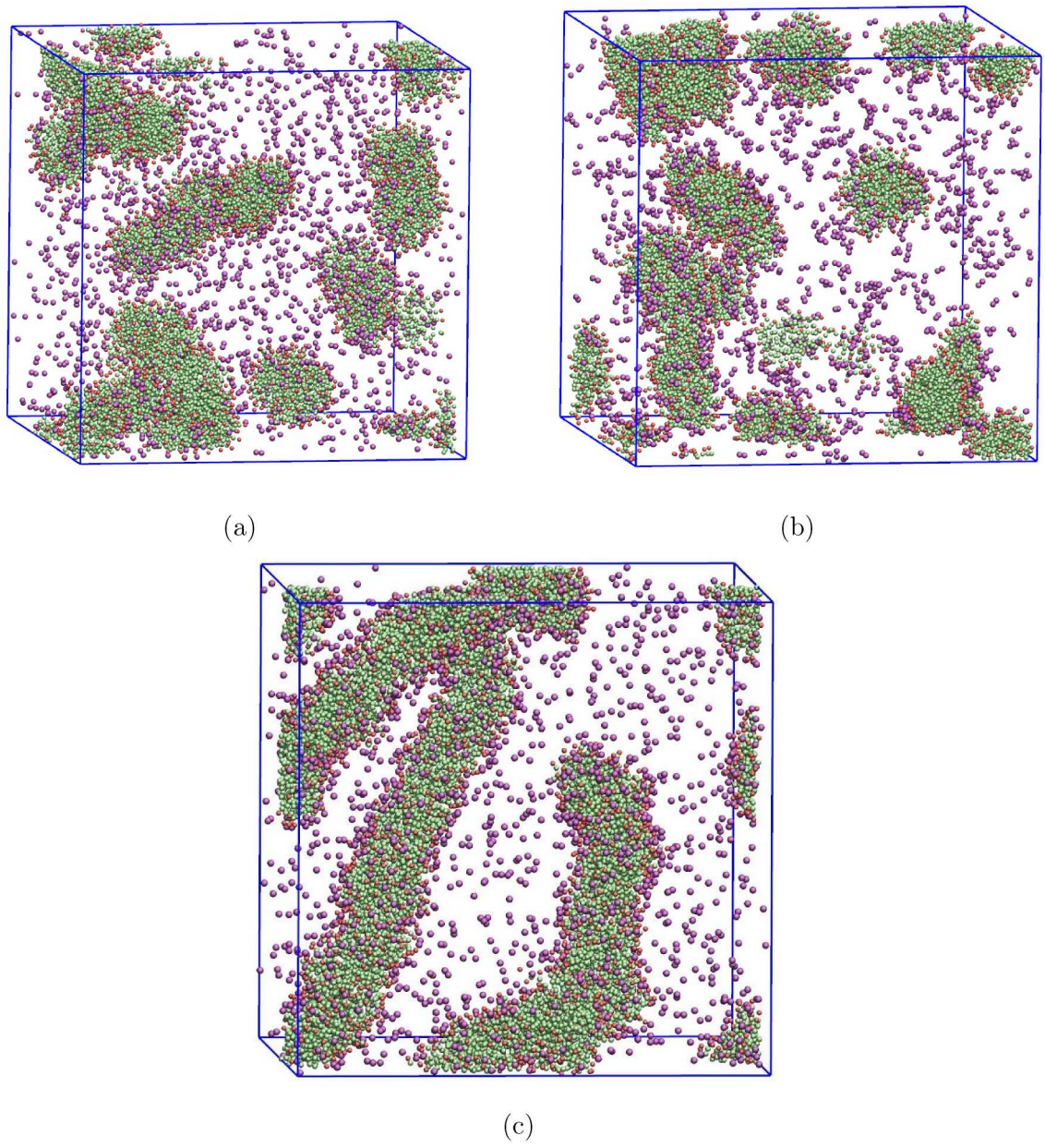

Figure 17. (Colour online) Simulation snapshots of the final configuration starting from a random configuration of surfactant, water and bromide counter-ions with neutral silica monomers (a), neutral silica dimers (b) and anionic silica monomers (c). CTA^+ head group beads are shown in red, tail group beads are shown in green and silica is shown in purple with bromide counter-ions and water beads hidden for clarity.

the number of silicate species was set so that the system contains an equal number of silicon atoms as surfactant molecules, which also results in a net zero charge without any counter-ions when fully deprotonated anionic silicates are used. For simulations with neutral silicates, bromide counter-ions are added. The concentration of surfactant used in all simulations for this section corresponds to the micellar region of the CTAB phase diagram (see Figure 16) and without the presence of silica should produce spherical and/or elongated micelles similar to those shown in Figure 15. All simulations started from a completely random arrangement of the molecules in the simulation box.

Firstly, neutral silicates were added to an initial random configuration of surfactant molecules. Snapshots of the final configurations achieved in self-assembly simulations involving neutral silicates (both monomers and dimers) are shown in Figure 17 (a and b). The configurations obtained in both cases are very similar to the control system without silicates present, suggesting that the presence of neutral silicates is not sufficient to promote aggregation of surfactant micelles, as expected.

Next, anionic silica monomers were added to an initial random configuration of surfactant molecules. The final configuration after 3 μs of simulation time is shown in Figure 17(c). The presence of anionic silicate monomers promotes the fusion of micelles to form long worm-like micelles. However, in agreement with previous simulation studies [9] and experimental observations [11], anionic silica monomers are not sufficient to promote phase separation and hexagonal phase formation at this concentration of surfactant. These

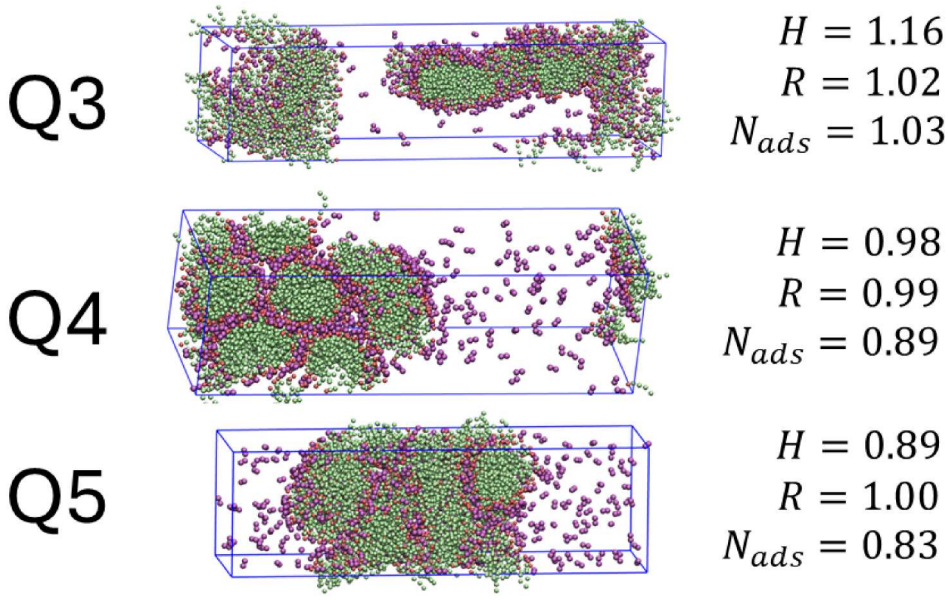

Figure 18. (Colour online) Simulation snapshots of the final configuration for a system containing CTA^+ and anionic silica dimers in water after 6 μs of simulation time using the Q3, Q4 and Q5 bead types to represent anionic silica beads. The colour code is the same as in Figure 17. The corresponding fitting parameters for these bead types are displayed alongside.

observations support the choice of bead type (Q2) made for anionic silica monomers. This also indicates that despite the differences in the atomistic models used for parameterisation in this work and in the previous work of Pérez-Sánchez et al. [9], resulting in monomers adsorbing outside the surfactant headgroup rather than being absorbed within the micelle surface, the self-assembly behaviour of CTAB in the presence of silica monomers is unchanged.

Previously, comparison against atomistic data for a single micelle identified that the correct bead type for anionic silica dimers lies in the range of Q3–Q5, with Q4 being selected as a good compromise. Therefore, it is important to test the sensitivity of the self-assembly results to this choice of bead. Hexagonal phases were observed to be formed experimentally in the presence of a distribution of silicate oligomers [11] and in previous simulation studies in the presence of both oligomers and dimers [10,12]. Therefore, we tested the ability of our new model to reproduce these observations in a solution of CTAB and anionic silica dimers. This initial test makes use of elongated simulation boxes which were used in previous work [10] in order to promote faster phase separation and organisation. A relatively high surfactant concentration (of 20 wt%) was used to ensure that the surfactant phase is large enough to show the periodicity of the HLC phase, whilst keeping the total simulation time small enough to reduce computational demand. Note that this is still within the micellar region of the pure CTAB phase diagram (Figure 16). Each simulation was carried out for 6 μs.

Simulation snapshots of the final configurations obtained for these initial tests are shown in Figure 18. For the Q3 bead type, the presence of dimers promotes the aggregation of surfactant micelles into rods, full phase separation does not occur and there is no evidence of HLC phase formation. This may be due to the Q3 bead resulting in a model for silica that is too hydrophobic with excessive adsorption of silica dimers at the interface between surfactant headgroup and water, preventing adequate aggregation of the surfactant phase. For the Q4 bead type, clear evidence of phase separation and HLC phase formation can be observed with several surfactant rods ordered in a 'honeycomb' arrangement. This provides strong evidence that the Q4 bead is the right choice for modelling silica dimers. For the Q5 bead type, while phase separation does occur in this case and some evidence of parallel ordered rods can be observed, the arrangement of these rods appears to be somewhat disordered. Compared with the Q4 bead, the Q5 bead is more hydrophilic, which results in a higher proportion of silica dimers remaining in the bulk water rather than adsorbing at the interface between surfactant headgroup and water. This may result in there being too few silicate species to permit the assembly of an ordered HLC phase. These results indicate that the bead type selection for representing silicates is critical to reproducing the co-operative templating phenomena observed in silica/surfactant/water systems.

For a more thorough validation, larger simulations using a rectangular, 'half cubic', box with dimensions of $31.6 \times 31.6 \times 15.8$ nm were carried out. The shorter dimension in the z direction allows the surfactant phase to more easily bridge periodic boundaries and promotes rod formation in a single direction whilst ensuring that the small simulation box size does not artificially produce periodic phases. This z dimension is large enough (many times larger than a surfactant micelle) to ensure rods that form are sufficiently long compared to their width. The final configuration of this simulation after approximately 24 μs is shown in Figure 19. The formation of a hexagonal phase made up of multiple parallel rods spanning the shorter z dimension is clearly visible. The progression of the simulation with time is also shown in Figure S4 in Supporting Information. Starting from a random arrangement of surfactant and silicate species dispersed in water, surfactants very quickly form micelles, which occurs

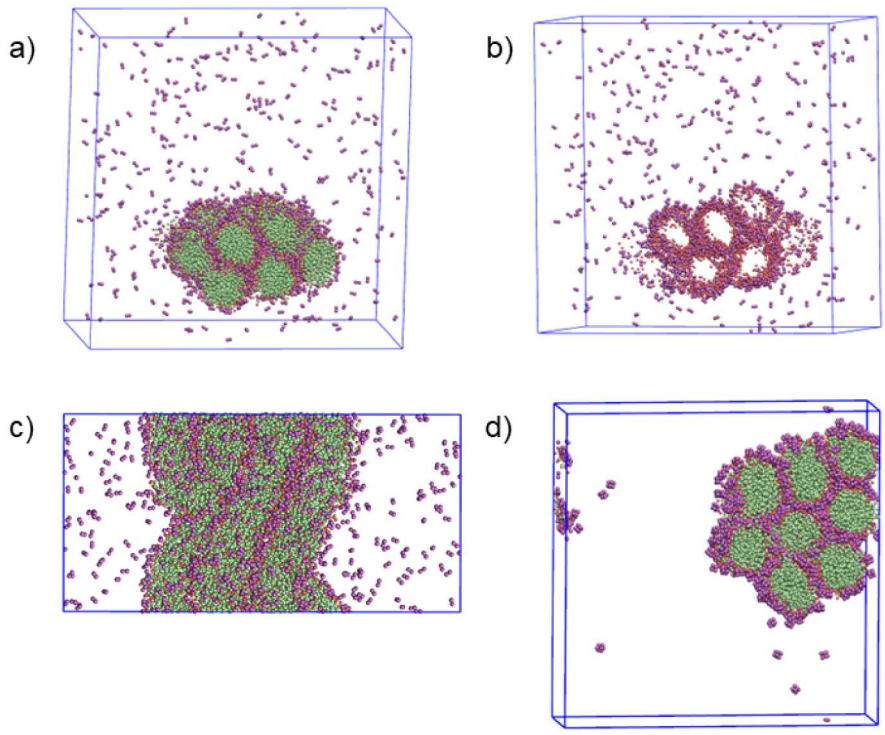

Figure 19. (Colour online) Simulation snapshots of the final configuration obtained using Q4 beads to represent silica oligomers. Panels (a)–(c) show a system containing anionic silica dimers while panel (d) shows a system containing anionic silica octamers with a −4 charge. Colour code is the same as in Figure 17. For snapshots of silica dimers, (a) shows the simulation from the positive z direction with all beads visualised, while (b) shows a cutaway of only silica and surfactant head beads and (c) shows a top-down view.

within 15 ns of simulation time. Silicates are attracted to the surface of micelles, screening the repulsive interactions between them and promoting the aggregation of micelles into several long worm-like micelles, which occurs approximately in the first 60 ns. The rod-like micelles then aggregate and phase separate, which is complete after approximately 600 ns. After this point, reorganisation of the surfactant phase into a more ordered HLC arrangement takes place, which is a much more lengthy process.

While the presence of anionic silica dimers has been demonstrated to be sufficient to promote the formation of the HLC phase, higher oligomers such as cubic octamers and cyclic trimers have been shown to promote HLC formation in prior computational work [10]. These larger oligomers are often more directly relevant to experimental systems; for example under the synthesis conditions of MCM-41 approximately 70% of silicate species are present as cubic octamers [11]. Therefore, a simulation was carried out to ensure that HLC formation is possible in the presence of these larger oligomers of silica. The final configuration after 3 μs is shown in Figure 19(d), revealing the formation of a very well-ordered phase-separated HLC.

4. Conclusions

In this work, we have presented a coarse-grained model that is able to describe the early stages of ordered mesoporous silica synthesis, capable of accurately representing the interactions of silica precursor species (monomeric and oligomeric silicates with a variety of sizes and charge states) in the presence of templating surfactant species. This coarse-grained model is the first to be calibrated against the atomistic model of Jorge et al., which provides improved interactions that are validated against experimental data [20]. It is based on the Martini 3 force-field [19], which offers several advantages over previous coarse-grained models. While this model is calibrated based on interactions with the popular cationic surfactant, CTAB, it can readily be extended to include other surfactant species that are compatible with the Martini 3 framework, by following the procedure for surfactant model development described here. The development of this model is supported by a robust multi-scale modelling methodology based on fitting parameters, which employs a rational approach to determining appropriate interaction parameters between inorganic precursor and templating species. This will aid future model development for similar systems as well as indicating how manipulation of these parameters affects self-assembly behaviour.

Self-assembly simulations of pure CTAB solutions, as well as CTAB/silica solutions, yielded results in excellent agreement with available experimental data. In particular, the experimental dependence of the CTAB aggregation number with concentration is captured accurately by our CG model, while the silica model can describe the formation of hexagonal mesophases under conditions observed experimentally. Neutral silicate species were observed to have very little influence on the surfactant self-assembly process, in agreement with previous observations that the degree of order of OMS-like materials decreases as the pH decreases due to the reduction in the ability of silicates to balance the charge around surfactant micelles

[60]. Anionic silica monomers, on the contrary, rapidly induced a sphere-to-rod transition in dilute surfactant solutions, again in agreement with experimental observations. Despite the fact that our new CG model for silica monomers (and, by implication, the atomistic model it was based on) is substantially more hydrophilic than previous models [9,13,14], this does not seem to affect the morphology or self-assembly mechanism of the worm-like micelles obtained in those solutions. Simulations of CTAB solutions with silica dimers and cubic octamers, representative of the early stages of OMS synthesis, confirmed the crucial role played by silica oligomers in promoting micelle aggregation into an ordered hexagonal array by acting as 'bridges' between different micelles.

One important limitation of our modelling approach, which it shares with the earlier model of Pérez-Sánchez et al. [10], is that silicates of multiple degrees of oligomerisation (i.e. monomers, dimers, octamers) are parametrised separately. These pre-formed oligomers can then be inserted into CG simulations directly, either at the start of the simulation to represent a single stage in the condensation process, or added throughout the simulation manually to represent gradually increasing oligomerisation. An alternative approach, which more realistically describes experimental mesoporous silica synthesis processes, is to implement a reactive model that explicitly describes silica polycondensation reactions, such as the model of Carvalho et al. [61]. In this case, only monomers need to be parametrised, as higher oligomers are simply represented by 'reactive potentials' between monomers. Although the reactive approach is more challenging to parametrise and significantly slows down the simulations, this represents a promising approach for future explorations of porous silica synthesis where the time scales of reaction and self-assembly are of similar magnitude.

Disclosure statement

No potential conflict of interest was reported by the author(s).

Funding

SP thanks funding from EPSRC grants (EP/P006892/1, EP/V051458/1, EP/R025983/1) to support this research. TS is grateful to EPSRC for a DTP studentship (EP/T517938/1, studentship ref. 2606787) and to the Department of Chemical and Biological Engineering at the University of Sheffield for financial support. Results were obtained using ARCHIE-WeSt High Performance Computer (www.archie-west.ac.uk) based at the University of Strathclyde.

Data availability statement

All data underpinning this publication are openly available from the University of Strathclyde KnowledgeBase at https://doi.org/10.15129/6f3b22a3-beb7-4d79-bf39-a8e521ed823d.

References

[1] Beck JS, Vartuli JC, Roth WJ, et al. A new family of mesoporous molecular sieves prepared with liquid crystal templates. J Am Chem Soc. 1992 Dec;114(27):10834–10843. doi: 10.1021/ja00053a020

[2] Croissant JG, Fatieiev Y, Almalik A. Mesoporous silica and organosilica nanoparticles: physical chemistry, biosafety, delivery strategies, and biomedical applications. Adv Healthc Mater. 2018;7(4):1700831. doi: 10.1002/adhm.v7.4

[3] Kumar P, Guliants V. Periodic mesoporous organic-inorganic hybrid materials: applications in membrane separations and adsorption. Micropor Mesopor Mat. 2010 Jul;132:1–14. doi: 10.1016/j.micromeso.2010.02.007

[4] Blin JL, Impéror-Clerc M. Mechanism of self-assembly in the synthesis of silica mesoporous materials: in situ studies by X-ray and neutron scattering. Chem Soc Rev. 2013 Apr;42(9):4071–4082. doi: 10.1039/C2CS35362H

[5] Jorge M, Milne AW, Sobek ON, et al. Modelling the self-assembly of silica-based mesoporous materials. Mol Simul. 2018 Apr;44(6):435–452. doi: 10.1080/08927022.2018.1427237

[6] Siperstein FR, Gubbins KE. Synthesis and characterization of templated mesoporous materials using molecular simulation. Mol Simul. 2001 Nov;27(5-6):339–352. doi: 10.1080/08927020108031357

[7] Siperstein FR, Gubbins KE. Phase separation and liquid crystal self-assembly in surfactant-inorganic-solvent systems. Langmuir. 2003 Mar;19(6):2049–2057. doi: 10.1021/la026410d

[8] Jin L, Auerbach SM, Monson PA. Simulating the formation of surfactant-templated mesoporous silica materials: a model with both surfactant self-assembly and silica polymerization. Langmuir. 2013 Jan;29(2):766–780. doi: 10.1021/la304475j

[9] Pérez-Sánchez G, Gomes JRB, Jorge M. Modeling self-assembly of silica/surfactant mesostructures in the templated synthesis of nanoporous solids. Langmuir. 2013 Feb;29(7):2387–2396. doi: 10.1021/la3046274

[10] Pérez-Sánchez G, Chien SC, Gomes JRB, et al. Multiscale model for the templated synthesis of mesoporous silica: the essential role of silica oligomers. Chem Mater. 2016 Apr;28(8):2715–2727. doi: 10.1021/acs.chemmater.6b00348

[11] Firouzi A, Atef F, Oertli AG, et al. Alkaline lyotropic silicate-surfactant liquid crystals. J Am Chem Soc. 1997 Apr;119(15):3596–3610. doi: 10.1021/ja963007i

[12] Chien SC, Pérez-Sánchez G, Gomes JRB, et al. Molecular simulations of the synthesis of periodic mesoporous silica phases at high surfactant concentrations. J Phys Chem C. 2017 Mar;121(8):4564–4575. doi: 10.1021/acs.jpcc.6b09429

[13] Jorge M, Gomes JRB, Cordeiro MNDS, et al. Molecular simulation of silica/surfactant self-assembly in the synthesis of periodic mesoporous silicas. J Am Chem Soc. 2007 Dec;129(50):15414–15415. doi: 10.1021/ja075070l

[14] Jorge M, Gomes JRB, Cordeiro MNDS, et al. Molecular dynamics simulation of the early stages of the synthesis of periodic mesoporous silica. J Phys Chem B. 2009 Jan;113(3):708–718. doi: 10.1021/jp806686w

[15] Pereira JCG, Catlow CRA, Price GD. Molecular dynamics simulation of methanolic and ethanolic silica-based sol-gel solutions at ambient temperature and pressure. J Phys Chem A. 2002 Jan;106(1):130–148. doi: 10.1021/jp010078h

[16] Gomes JRB, Cordeiro MNDS, Jorge M. Gas-phase molecular structure and energetics of anionic silicates. Geochim Cosmochim Acta. 2008 Sep;72(17):4421–4439. doi: 10.1016/j.gca.2008.06.012

[17] Marrink SJ, Risselada HJ, Yefimov S, et al. The MARTINI force field: coarse grained model for biomolecular simulations. J Phys Chem B. 2007 Jul;111(27):7812–7824. doi: 10.1021/jp071097f

[18] Alessandri R, Souza PCT, Thallmair S, et al. Pitfalls of the martini model. J Chem Theory Comput. 2019 Oct;15(10):5448–5460. doi: 10.1021/acs.jctc.9b00473

[19] Souza PCT, Alessandri R, Barnoud J, et al. Martini 3: a general purpose force field for coarse-grained molecular dynamics. Nat Methods. 2021 Apr;18(4):382–388. doi: 10.1038/s41592-021-01098-3

[20] Jorge M, Milne AW, Barrera MC, et al. New Force-Field for organosilicon molecules in the liquid phase. ACS Phys Chem Au. 2021 Nov;1(1):54–69. doi: 10.1021/acsphyschemau.1c00014

[21] Jorge M. New united-atom model for alkanes, alkenes, and alkynes. J Comput Chem. 2017;38(6):359–369. doi: 10.1002/jcc.v38.6

[22] Barrera MC, Jorge M. A polarization-consistent model for alcohols to predict solvation free energies. J Chem Inf Model. 2020 Mar;60(3):1352–1367. doi: 10.1021/acs.jcim.9b01005

[23] Iler RK. The chemistry of silica: solubility, polymerization, colloid and surface properties and biochemistry of silica. New York: Wiley; 1979.
[24] Sefcík J, McCormick AV. Thermochemistry of aqueous silicate solution precursors to ceramics. AIChE J. 1997;43(S11):2773–2784. doi: 10.1002/(ISSN)1547-5905
[25] Graham JA, Essex JW, Khalid S. PyCGTOOL: automated generation of coarse-grained molecular dynamics models from atomistic trajectories. J Chem Inf Model. 2017 Apr;57(4):650–656. doi: 10.1021/acs.jcim.7b00096
[26] Berendsen HJC, van der Spoel D, van Drunen R. GROMACS: a message-passing parallel molecular dynamics implementation. Comput Phys Commun. 1995 Sep;91(1):43–56. doi: 10.1016/0010-4655(95)00042-E
[27] Lindahl AH. GROMACS 2021.5 Source code; 2022.
[28] Van Rossum G, Drake FL. Python 3 reference manual. Scotts Valley, CA: CreateSpace; 2009.
[29] Michaud-Agrawal N, Denning EJ, Woolf TB, et al. MDAnalysis: a toolkit for the analysis of molecular dynamics simulations. J Comput Chem. 2011;32(10):2319–2327. doi: 10.1002/jcc.v32.10
[30] Gowers RJ, Linke M, Barnoud J, et al. MDAnalysis: a python package for the rapid analysis of molecular dynamics simulations. Proc Python Sci Conf. 2016;98–105. doi: 10.25080/issn.2575-9752
[31] Hunter JD. Matplotlib: A 2D graphics environment. Comput Sci Eng. 2007;9(3):90–95. doi: 10.1109/MCSE.2007.55
[32] Hockney RW, Goel SP, Eastwood JW. Quiet high-resolution computer models of a plasma. J Comput Phys. 1974 Feb;14(2):148–158. doi: 10.1016/0021-9991(74)90010-2
[33] Bussi G, Donadio D, Parrinello M. Canonical sampling through velocity rescaling. J Chem Phys. 2007 Jan;126(1):014101. doi: 10.1063/1.2408420
[34] Parrinello M, Rahman A. Polymorphic transitions in single crystals: a new molecular dynamics method. J Appl Phys. 1981 Dec;52(12):7182–7190. doi: 10.1063/1.328693
[35] Nosé S, Klein ML. Constant pressure molecular dynamics for molecular systems. Mol Phys. 2006 Aug;50(5):1055–1076.
[36] Darden T, York D, Pedersen L. Particle mesh Ewald: an N.log(N) method for Ewald sums in large systems. J Chem Phys. 1993 Jun;98(12):10089–10092. doi: 10.1063/1.464397
[37] Essmann U, Perera L, Berkowitz M, et al. A smooth particle mesh Ewald method. J Chem Phys. 1995 Nov;103:8577–8593 doi: 10.1063/1.470117
[38] Berendsen HJC, Grigera JR, Straatsma TP. The missing term in effective pair potentials. J Phys Chem. 1987 Nov;91(24):6269–6271. doi: 10.1021/j100308a038
[39] Kaminski GA, Friesner RA, Tirado-Rives J, et al. Evaluation and reparametrization of the OPLS-AA force field for proteins via comparison with accurate quantum chemical calculations on peptides. J Phys Chem B. 2001 Jul;105(28):6474–6487. doi: 10.1021/jp003919d
[40] Watkins EK, Jorgensen WL. Perfluoroalkanes: conformational analysis and liquid-state properties from ab initio and Monte Carlo calculations. J Phys Chem A. 2001 Apr;105(16):4118–4125. doi: 10.1021/jp004071w
[41] Price MLP, Ostrovsky D, Jorgensen WL. Gas-phase and liquid-state properties of esters, nitriles, and nitro compounds with the OPLS-AA force field. J Comput Chem. 2001;22(13):1340–1352. doi: 10.1002/jcc.v22:13
[42] Rizzo RC, Jorgensen WL. OPLS All-Atom model for amines: resolution of the amine hydration problem. J Am Chem Soc. 1999 May;121(20):4827–4836. doi: 10.1021/ja984106u
[43] Jorgensen WL, McDonald NA. Properties of liquid pyridine and diazenes. J Mol Struct THEOCHEM. 1998 Feb;424(1-2):145–155. doi: 10.1016/S0166-1280(97)00237-6
[44] Jorgensen WL, Maxwell DS, Tirado-Rives J. Development and testing of the OPLS all-atom force field on conformational energetics and properties of organic liquids. J Am Chem Soc. 1996 Nov;118(45):11225–11236. doi: 10.1021/ja9621760
[45] Verlet L. Computer 'Experiments' on classical fluids. I. Thermodynamical properties of Lennard-Jones molecules. Phys Rev. 1967 Jul;159(1):98–103. doi: 10.1103/PhysRev.159.98
[46] Hansson P, Jönsson B, Ström C, et al. Determination of micellar aggregation numbers in dilute surfactant systems with the fluorescence quenching method. J Phys Chem B. 2000 Apr;104(15):3496–3506. doi: 10.1021/jp992444r
[47] Aswal VK, Goyal PS. Role of different counterions and size of micelle in concentration dependence micellar structure of ionic surfactants. Chem Phys Lett. 2003 Jan;368(1-2):59–65. doi: 10.1016/S0009-2614(02)01833-X
[48] Hess B, Bekker H, Berendsen HJC, et al. LINCS: a linear constraint solver for molecular simulations. J Comput Chem. 1997;18(12):1463–1472. doi: 10.1002/(ISSN)1096-987X
[49] Melo MN, Ingólfsson HI, Marrink SJ. Parameters for Martini sterols and hopanoids based on a virtual-site description. J Chem Phys. 2015 Dec;143(24):243152. doi: 10.1063/1.4937783
[50] Thomasen FE, Skaalum T, Kumar A, et al. Rescaling protein-protein interactions improves Martini 3 for flexible proteins in solution. Nat Commun. 2024 Aug;15(1):6645. doi: 10.1038/s41467-024-50647-9
[51] Berr S, Jones RRM, Johnson JS. Effect of counterion on the size and charge of alkyltrimethylammonium halide micelles as a function of chain length and concentration as determined by small-angle neutron scattering. J Phys Chem. 1992 Jun;96(13):5611–5614. doi: 10.1021/j100192a075
[52] Quirion F, Magid LJ. Growth and counterion binding of cetyltrimethylammonium bromide aggregates at 25.degree.C: a neutron and light scattering study. J Phys Chem. 1986 Oct;90(21):5435–5441. doi: 10.1021/j100412a108
[53] Ležaic AMJ, Pejic N, Goronja J, et al. Micellar properties of cetyltrimethylammonium bromide in an acetonitrile-water mixture: conductometric and fluorescence studies. Maced J Chem Chem Eng. 2021 Nov;40(2):277–287. doi: 10.20450/mjcce.2021.2394
[54] Banjare RK, Banjare MK, Behera K, et al. Deep eutectic solvents as modulator on the micellization behaviour of cationic surfactants and potential application in human serum albumin aggregation. J Mol Liq. 2021 Dec;344:117864. doi: 10.1016/j.molliq.2021.117864
[55] Banjare RK, Banjare MK, Panda S. Effect of acetonitrile on the colloidal behavior of conventional cationic surfactants: a combined conductivity, surface tension, fluorescence and FTIR study. J Solution Chem. 2020 Jan;49(1):34–51. doi: 10.1007/s10953-019-00937-4
[56] Lianos P, Zana R. Fluorescence probe studies of the effect of concentration on the state of aggregation of surfactants in aqueous solution. J Colloid Interface Sci. 1981 Nov;84(1):100–107. doi: 10.1016/0021-9797(81)90263-0
[57] Ekwall P, Mandell L, Solyom P. The aqueous cetyl trimethylammonium bromide solutions. J Colloid Interface Sci. 1971 Apr;35(4):519–528. doi: 10.1016/0021-9797(71)90210-4
[58] Somasundaran P. Encyclopedia of surface and colloid science, 2004 update supplement. Boca Raton: CRC Press; 2004.
[59] Mokaya R. Mesoporous Materials, Synthesis and Properties. In: Meyers RA, editor. Encyclopedia of physical science and technology. 3rd ed. New York: Academic Press; 2003. p. 369–381.
[60] Centi A, Manning JRH, Srivastava V, et al. The role of charge-matching in nanoporous materials formation. Mater Horiz. 2019 Jun;6(5):1027–1033. doi: 10.1039/C8MH01640B
[61] Carvalho AP, Santos SM, Pérez-Sánchez G, et al. Sticky-MARTINI as a reactive coarse-grained model for molecular dynamics simulations of silica polymerization. Npj Comput Mater. 2022 Mar;8(1):1–13. doi: 10.1038/s41524-022-00722-w